

Interfacial Mixing Effect in a Promising Skyrmionic Material: Ferrimagnetic Mn_4N

Chung T. Ma,¹ Wei Zhou,¹ Brian J. Kirby,² and S. Joseph Poon^{1,3}

¹*Department of Physics, University of Virginia, Charlottesville, Virginia, 22904, USA*

²*NIST Center for Neutron Research, National Institute of Standards and Technology, Gaithersburg, Maryland 20899, USA*

³*Department of Materials Science and Engineering, University of Virginia, Charlottesville, Virginia, 22904, USA*

(*Electronic mail: ctm7sf@virginia.edu)

(Dated: 5 August 2022)

Interfacial mixing of elements is a well-known phenomenon found in thin film deposition. For thin-film magnetic heterostructures, interfacial compositional inhomogeneities can have drastic effects on the resulting functionalities. As such, care must be taken to characterize the compositional and magnetic properties of thin films intended for device use. Recently, ferrimagnetic Mn_4N thin films have drawn considerable interest due to exhibiting perpendicular magnetic anisotropy, high domain-wall mobility, and good thermal stability. In this study, we employed X-ray photoelectron spectroscopy (XPS) and polarized neutron reflectometry (PNR) measurements to investigate the interfaces of an epitaxially-grown $\text{MgO}/\text{Mn}_4\text{N}/\text{Pt}$ trilayer deposited at 450 °C. XPS revealed the thickness of elemental mixing regions of near 5 nm at both interfaces. Using PNR, we found that these interfaces exhibit essentially zero net magnetization at room temperature. Despite the high-temperature deposition at 450 °C, the thickness of mixing regions is comparable to those observed in magnetic films deposited at room temperature. Micromagnetic simulations show that this interfacial mixing should not deter the robust formation of small skyrmions, consistent with a recent experiment. The results obtained are encouraging in terms of the potential of integrating thermally stable Mn_4N into future spintronic devices.

I. INTRODUCTION

The interface plays an important role in the properties of thin-film heterostructures. For magnetic materials, many well-studied and important phenomena arise from interfacial effects, such as interfacial magnetic anisotropy¹⁻⁴, RKKY coupling in a synthetic antiferromagnet through a metal spacer⁵⁻⁸, and the interfacial Dzyaloshinskii-Moriya interaction (I-DMI)⁹⁻¹⁴. Furthermore, it has been reported that in many of these heterostructures, interfacial mixing and dead layers exist at the interfaces of magnetic and non-magnetic layers. Such interfacial compositional heterogeneities have led to varying magnetic properties, such as thickness-dependent anisotropy and magnetization¹⁵⁻²¹. These present challenges in fabricating and developing devices with magnetic thin films, such as magnetic tunnel junctions²². Therefore, investigating the effects due to interfacial mixing in heterostructures is a crucial step in designing new materials for spintronics applications.

Mn_4N thin films have recently garnered much attention in the spintronic community²³. Mn_4N forms an anti-perovskite crystal structure²⁴. It is a ferrimagnetic metal with a Curie temperature of 710 K²⁵. Experiments have shown that Mn_4N exhibits perpendicular magnetic anisotropy (PMA)²⁶⁻³² that is desirable for use as free and fixed layers in magnetic devices. Furthermore, these properties are resilient to high temperatures, at least up to 450 °C. More recently, tunable magnetic skyrmions have been reported to be present in $\text{MgO}/\text{Mn}_4\text{N}/\text{Pt}_x\text{Cu}_{1-x}$ thin films³³ wherein $\text{Pt}_x\text{Cu}_{1-x}$ is designed to provide a variable I-DMI that controls the size of the skyrmion. As such, Mn_4N can potentially be used as a building block in skyrmion-based memory devices. Nonethe-

less, in view of elemental mixing that tends to occur at the interfaces of thin-film heterostructures, the question remains as to what extent high-temperature deposition Mn_4N ²⁶⁻³² would adversely affect the functionalities of the Mn_4N based heterostructures. For example, the interface is known to play a significant role in the effectiveness of spin currents and spin-orbit torque between magnetic and non-magnetic layers³⁴⁻³⁷. In a recent study, Mn_4N has been reported to have a 2 nm mixing layer from transmission electron microscopy³⁰. Thus, further quantitative studies of the interfacial properties of Mn_4N based heterostructure films is pivotal in exploring the feasibility of using Mn_4N in future devices.

In this study, we investigated the interfaces of epitaxially-grown $\text{MgO}/\text{Mn}_4\text{N}$ (17 nm)/Pt films, which were deposited at the same time, using X-ray photoelectron spectroscopy (XPS) and polarized neutron reflectometry (PNR). From XPS, mixing layers were revealed at both $\text{MgO}/\text{Mn}_4\text{N}$ and $\text{Mn}_4\text{N}/\text{Pt}$ interfaces. At the $\text{MgO}/\text{Mn}_4\text{N}$ interface, an oxidation layer of 5 nm thick MgMnNO mixing layer was revealed. At the $\text{Mn}_4\text{N}/\text{Pt}$ interface, a 5 nm thick MnPtNO mixing layer was found. Analysis of the PNR data revealed that both top and bottom mixing layers exhibit essentially zero magnetization. The 5 nm thickness of the mixed layer at the $\text{MgO}/\text{Mn}_4\text{N}$ interface is comparable to other room temperature depositions^{19,20}, despite Mn_4N being deposited at 450 °C. Equally important, micromagnetic simulations presented herein show that even with the presence of mixing layers, magnetic skyrmions, which arise from I-DMI, are found to be stable in $\text{MgO}/\text{Mn}_4\text{N}/\text{Pt}_x\text{Cu}_{1-x}$ thin films. This finding is consistent with recent experimental results. All these findings indicate that Mn_4N is a promising material for designing skyrmion-based memory.

II. METHOD

We deposited 17 nm thick Mn_4N films on MgO substrates using a single Mn target by reactive radio frequency (rf) sputtering. The MgO substrates were wet-cleaned and heat-treated ex-situ³². The base pressure was 9 μPa . Sputter deposition was carried out at 450 $^\circ\text{C}$ and under an $\text{Ar}:\text{N}_2$ gas flow ratio of 93:7. A Pt capping layer was deposited at room temperature to prevent oxidation. Our previous work showed epitaxially growth $\text{MgO}/\text{Mn}_4\text{N}/\text{Pt}$ through X-ray diffraction (XRD)³²

We performed X-ray photoelectron spectroscopy (XPS) measurements to obtain the compositional depth profile using the PHI VersaProbe III XPS instrument (Note: Certain commercial equipment is identified in this paper to foster understanding. Such identification does not imply recommendation or endorsement by NIST, nor does it imply that the materials or equipment identified are necessarily the best available for the purpose). XPS data were collected after sputtering off a few layers from the surface. Each sputtering lasted about 15 seconds, and the total sputtering time was 10 minutes. We analyzed the XPS results based on the following model with three assumptions. First, the composition from an XPS measurement is the averaged composition of a 3 nm layer from the surface, and the measurement sensitivity is the same within the 3 nm layer. Second, the distribution of Mn_4N near the $\text{Mn}_4\text{N}/\text{Pt}$ and $\text{Mn}_4\text{N}/\text{MgO}$ surfaces follows the cumulative distribution function (CDF) of a Gaussian as below.

$$CDF(z; s, \sigma) = \frac{1}{\sigma\sqrt{2\pi}} \int_{-\infty}^z e^{-\frac{(t-s)^2}{2\sigma^2}} dt \quad (1)$$

where z is the distance from the MgO substrate, s is the interface boundary and σ is the thickness of the mixing.

Third, the distribution of the MnO is a Gaussian function (G) as below.

$$G(z; w, l, \sigma) = \frac{w}{\sigma\sqrt{2\pi}} e^{-\frac{(z-l)^2}{2\sigma^2}} \quad (2)$$

where w is the weight coefficient, l is the location of the MnO layers.

TABLE I. The distribution functions of each layer used in XPS fitting, where CDF is the cumulative distribution function of a Gaussian distribution, G is the Gaussian function, and A, B, C, D, E are normalization coefficients.

Layer	Distribution function
Pt	A(t) CDF($z; s_1, \sigma_1$)
MnO at $\text{Mn}_4\text{N}/\text{Pt}$	B(t) G($z; w, l_4, \sigma_4$)
Mn_4N	C(t) CDF($z; s_2, \sigma_2$)[1- CDF($z; s_1, \sigma_1$)]
MnO at $\text{MgO}/\text{Mn}_4\text{N}$	D(t) G($z; w, l_5, \sigma_5$)
MgO	E(t) CDF($z; s_3, \sigma_3$)

Table 1 summarizes the distribution of each layer, where A, B, C, D, E are normalization coefficients. Using this model, we calculated the averaged compositions $f_{avr}(z)$ at location

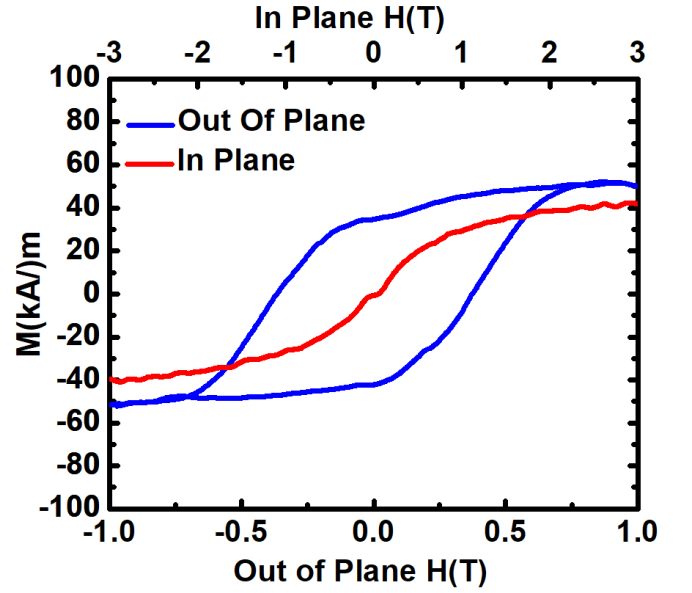


FIG. 1. Magnetic hysteresis loops of 17 nm thick Mn_4N at room temperature. The out-of-plane loop (blue) shows a coercivity of 0.5 T and the in-plane loop (grey) shows an anisotropy field over 3 T. (1 T = 10000 Oe / μ_0)

z by integrating the distribution from $z - 3$ nm to z and fitted these $f_{avr}(z)$ with the composition obtained from the XPS measurement by tuning parameters in CDF and G.

Polarized neutron reflectometry (PNR) measurements were performed at room temperature in a 3 T in-plane field using the PBR instrument at the NIST Center for Neutron Research. The reflectivities were measured as a function of the wavevector Q along the normal direction to the sample surface (i.e. specular scattering). Data were reduced and model-fitted with the reductus³⁸ and Refl1D³⁹ software packages, respectively. The modeling allowed us to deduce the depth profiles of the film's nuclear scattering length density (ρ_N , indicative of the nuclear composition), and the in-plane magnetization⁴⁰.

Micromagnetic simulations of Mn_4N were carried out using the Object-Oriented Micromagnetic Framework⁴¹. Details of the simulations can be found in a previous publication³³. The simulation dimensions are 300 x 300 x 15 nm, and each cell is 5 x 5 x 5 nm. The exchange stiffness constant between each cell is 1.5×10^{-11} J/m. The external field is 0.01 T. The anisotropy (K_u) is $(0.5 - 1.2) \times 10^5$ J/m³. We added a 5 nm thick magnetically dead layer at the $\text{Mn}_4\text{N}/\text{Pt}$ interface, which is assumed to provide a DMI according to the fractional composition of Pt in the layer but no magnetic interaction. Skyrmion size is defined as the average diameter of a boundary with zero magnetizations.

III. RESULTS AND DISCUSSION

Figure 1 shows the hysteresis loops of Mn_4N at 300 K. The out-of-plane and in-plane $M(H)$ loops confirm perpendicular magnetic anisotropy (PMA). The coercivity is found to

be about 0.55 T, and saturation magnetization is 40 x kA/m. From the in-plane loop, the anisotropy field is determined to be over 3 T. The in-plane magnetization remains unsaturated at 3 T, which is the limit of the equipment. Using these results, the anisotropy (K_u) is estimated to exceed 70 kJ/m³, comparable to other studies^{26–32}. Figure 2 shows (a) the compositional depth profile, and (b) the first derivative of the compositional depth profile, as a function of distance from the MgO substrate as determined from XPS. The surface of the MgO substrate is ideally set at $z = 0$ nm. In view of the presence of an interfacial layer, $z = 0$ nm is set at the position where the relative composition of Mg and O is 1:1. As such, $z = 0$ nm is the beginning of the MgO/Mn₄N interface region. The bulk of the Mn₄N layer is seen to extend to around 20 nm. Above approximately $z = 20$ nm is the Mn₄N/Pt interface region. From Figure 2 (a), elemental mixings exist at both MgO/Mn₄N and Mn₄N/Pt interface. At the MgO/Mn₄N interface region ($z = 0$ nm), both Mg and O atoms from the MgO substrate diffuse into Mn₄N. Since Mn reacts easily with O, but not Mg, O diffuses further into Mn₄N. Overall, the nominal average composition of this interface region is Mg₂₀O₃₇Mn₃₇N₆. From Figure 2 (b), the first derivative of the fitted compositional depth profile verifies that O diffuses further into the Mn₄N layer, as indicated by the peak of O occurring at higher z than that of Mg. Furthermore, the thickness of this interface region can be estimated using the full width at half maximum of the derivative. The mixing region with Mn₄N and MgO is about 5 nm thick, with O diffuses about 3 nm further into Mn₄N. The presence of this interfacial layer at the MgO/Mn₄N interface is possibly due to rough MgO/Mn₄N interfaces. From Shen et al.⁴², misfit dislocations were observed by transmission electron microscopy, while such dislocations were not found at STO/Mn₄N interface²³.

Both the Mn and N distributions shown in the composition derivative plot are separated by about 17 nm, which is the nominal thickness of the Mn₄N layer. It is worth noting that a small amount of O exists in the region. This is possibly due to the presence of O during the deposition. Even though the base pressure is below 9 μ Pa, and only Ar:N₂ was used, very tiny amounts of O can enter the system through the Ar or N₂ gas feed lines. Since Mn reacts easily with O, O enters Mn₄N. Overall, the composition of this region is Mn_{77.7}N_{19.6}O_{2.7}. This means that Mn:N maintains 4:1 in this sample, despite the presence of O. Above Mn₄N ($z > 20$ nm) lies the region of the Mn₄N/Pt interface. Both Pt and O atoms are found to diffuse into Mn₄N. The nominal average composition of this interface region is Mn₃₇N₆O₂₀Pt₃₇. The increase of O content at the Mn₄N/Pt interface is possibly due to the extended time required to cool down before room temperature deposition of Pt with trace amounts of O in the system. Using the full width at half maximum of Pt composition derivative in Figure 2 (b), this region is about 5 nm thick. It is worth noting that the mixing regions at both interfaces are about 5 nm thick, even though one was deposited at 450 °C and Pt was deposited at room temperature.

To understand the magnetic consequences of the compositional inhomogeneity, we characterized the magnetization depth profile with PNR. Figure 3 (a) shows the model-

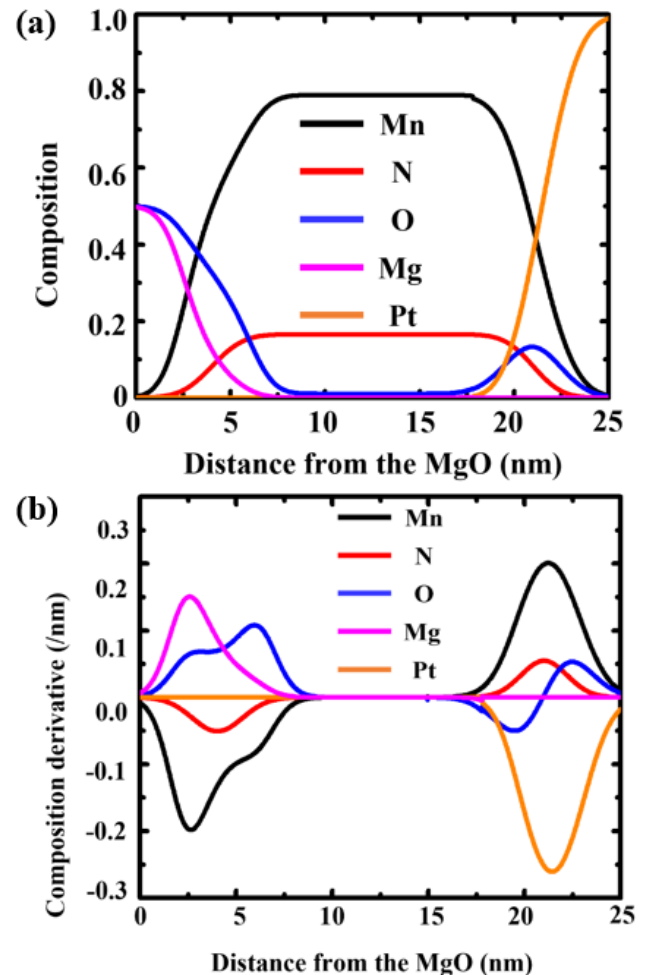


FIG. 2. (a) Compositional depth profile of MgO (001)/Mn₄N/Pt obtained from X-ray photoelectron spectroscopy (XPS) by fitting as a function of distance from MgO substrate. 0 nm is the surface of the MgO substrate. The fitted depth profile shows mixings at both MgO (001)/Mn₄N and Mn₄N/Pt interface. (b) First derivative of the fitted depth profile of MgO (001)/Mn₄N/ as a function of distance from MgO substrate.

fitted spin-dependent reflectivities ($++$ and $-$) as functions of wavevector transfer Q . The data show clear oscillations, demonstrating sensitivity to the scattering length density depth profile. However, the scattering is dominated by nuclear contributions, as the difference between $++$ and $-$ is essentially too small to detect in (a). In Fig. 3 (b) the same fitted data are plotted as spin-asymmetry (SA, difference in $++$ and $-$ divided by the sum) which highlights magnetic contributions to the scattering. Shown in this way, a spin-dependent signal is evident, demonstrating sensitivity to a non-zero magnetic depth profile. Fig. 3(c) shows the magnetic and nuclear profiles corresponding to the best fit shown in panels (b) and (c). In this model, the compositional profile of the nominal Mn₄N layer determined from XPS is approximated in terms of a 3 sublayer structure smeared out by error function roughness⁴³ accounting for both conven-

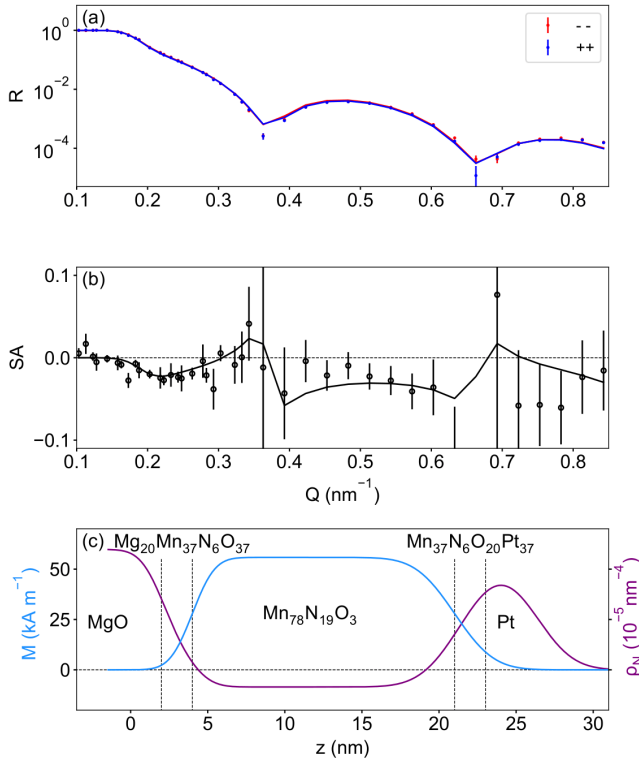


FIG. 3. (a) Model-fitted spin-dependent neutron reflectivities, R_{++} (blue) and R_{--} (red) measure at room temperature in 3 T. (b) Fitted data from (a) plotted as spin asymmetry to highlight the spin dependence. (c) In-plane magnetization (blue) and nuclear scattering length density (purple) depth profiles. Error bars in (a-b) correspond to 1 standard deviation.

tional interlayer roughness and compositional gradients: $\text{MgO} / \text{Mg}_{20}\text{O}_{37}\text{Mn}_{37}\text{N}_6 / \text{Mn}_{78}\text{N}_{19}\text{O}_3 / \text{Mn}_{37}\text{N}_6\text{O}_{20}\text{Pt}_{37} / \text{Pt}$. All nuclear scattering length densities were calculated based on the expected composition and were treated as fixed parameters in the fitting. $\text{Mg}_{20}\text{O}_{37}\text{Mn}_{37}\text{N}_6$ and $\text{Mn}_{37}\text{N}_6\text{O}_{20}\text{Pt}_{37}$ sublayer thicknesses were held fixed at 2 nm, and the Pt cap layer thickness was fixed at 3 nm. Interlayer roughness was assumed to be equal for all interfaces, and it was found to be 1 nm. The $\text{Mn}_{78}\text{N}_{19}\text{O}_3$ layer thickness was a free parameter, found to be 17 nm, confirming XPS results. The magnetizations of all 3 sublayers of the nominal Mn_4N layer were treated as free parameters. The profile shows a center $\text{Mn}_{78}\text{N}_{19}\text{O}_3$ layer magnetization of 56 kA/m , with a sharp decline near both interfaces. While the magnetization does not go completely to zero in the interfacial sublayer regions, this is consistent with layers of zero magnetization smeared out by the apparent roughness⁴⁴. The integrated magnetization for the entirety of the nominal Mn_4N film is 45 kA/m , consistent with the magnetometry data shown in Fig. 1. Despite the rigid constraints, Fig. 3 (a-b) show that this model gives an excellent fit to the data, and we note that models with a uniform magnetization profile in the nominal Mn_4N layer result in a significantly worse fit. Thus, the PNR results confirm the compositional profile determined from XPS, and show that the interfaces

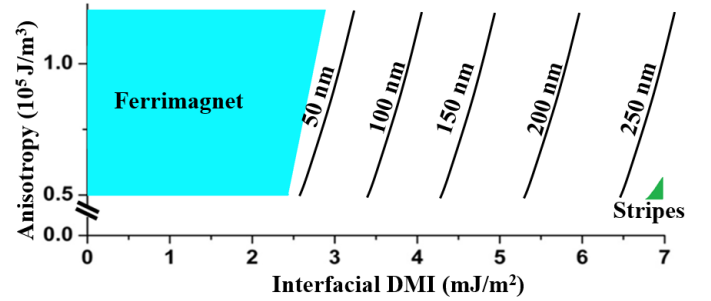


FIG. 4. Micromagnetic simulation of skyrmions in 15 nm Mn_4N with 5 nm of magnetic dead layer separated the interface and the Mn_4N sample at 300 K. Anisotropy (K_u) varies from 0.5 to $1.2 \times 10^5 \text{ J/m}^3$. Interfacial DMI varies from 0 to 7 mJ/m^2 . The blue region corresponds to ferrimagnetic states. Black lines correspond to the size of skyrmions in Mn_4N . The green region corresponds to larger than 250 nm skyrmions which form into stripes because of the limited simulated space of $300 \text{ nm} \times 300 \text{ nm}$ used.

of the nominal Mn_4N layers contribute no net magnetization. This finding is crucial in designing spintronics devices with Mn_4N . With non-magnetic interfacial mixings, these regions can be treated as a non-magnetic layer for the effectiveness of spin currents and spin-orbit torque in Mn_4N heterostructures. Thus, Mn_4N remains a viable option for future devices.

Micromagnetic simulations are employed to study the effect of interfacial mixings on skyrmion formation in Mn_4N . Figure 4 shows the DMI- K_u phase diagram of a 15 nm thick Mn_4N with a 5 nm thick magnetic dead layer at 300 K. Only the $\text{Mn}_4\text{N}/\text{Pt}$ mixing region is considered here. In the $\text{MgO}/\text{Mn}_4\text{N}/\text{Pt}$ heterostructure, interfacial-DMI is dominated by Pt, so a magnetic dead layer at $\text{Mn}_4\text{N}/\text{Pt}$ can potentially influence skyrmion formation. From XPS, this region has an average composition of $\text{Mn}_{37}\text{N}_6\text{O}_{20}\text{Pt}_{37}$. From density functional theory (DFT) calculations, interfacial-DMI at $\text{Mn}_4\text{N}/\text{Pt}$ is near 17 mJ/m^2 . Using a simple fractional composition model, this region is estimated to have a DMI of 2.6 mJ/m^2 . On the other hand, little or no effect is expected for the $\text{MgO}/\text{Mn}_4\text{N}$ as the interfacial-DMI is negligible between MgO and Mn ³³. Thus, this region is treated as a non-interacting empty space. Using experimental K_u of $0.7 \times 10^5 \text{ J/m}^3$, robust skyrmions are observed in interfacial-DMI above 2.5 mJ/m^2 . Below this DMI, only ferrimagnetic states are observed. With interfacial-DMI of 3.5 mJ/m^2 , near 100 nm skyrmions are found in Mn_4N . As interfacial-DMI increases to 5.5 mJ/m^2 , skyrmion sizes increase to 200 nm . At interfacial-DMI close to 7.0 mJ/m^2 , 250 nm skyrmions are observed in the simulations. With larger interfacial-DMI, skyrmions start to evolve into stripes. However, this phenomenon could be due to the limit of the simulation space of 300 nm in the in-plane direction.

From Figure 4, using experimental K_u of 0.7 mJ/m^3 and calculated interfacial-DMI at $\text{Mn}_4\text{N}/\text{Pt}$ of 17 mJ/m^2 , skyrmions are just over 250 nm in size. This is comparable to the observed skyrmions in $\text{MgO}/\text{Mn}_4\text{N}/\text{Pt}$, which range from 250 nm to 350 nm in size. Furthermore, from experiment, skyrmions in $\text{MgO}/\text{Mn}_4\text{N}/\text{Pt}_{0.1}\text{Cu}_{0.9}$ are around

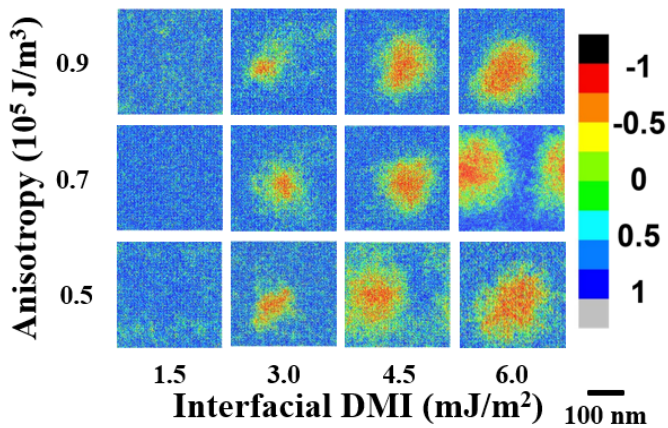


FIG. 5. Color mapping of out-of-plane magnetization in 15 nm Mn_4N with magnetically dead layers at 300 K from micromagnetic simulation. Red regions correspond to down magnetic moments and blue regions correspond to up magnetic moments.

100 nm. From DFT calculation, the interfacial-DMI of $\text{Cu}/\text{Mn}_4\text{N}$ is 2.6 mJ/m^2 ²³³. Assuming a simple solution model, the interfacial-DMI of $\text{Mn}_4\text{N}/\text{Pt}_{0.1}\text{Cu}_{0.9}$ is estimated to be 3.0 mJ/m^2 . From Figure 4, with K_u of 0.7 mJ/m^3 and interfacial-DMI of 3.0 mJ/m^2 , skyrmions are about 60 nm in diameter. This is smaller than the measured skyrmions in $\text{MgO}/\text{Mn}_4\text{N}/\text{Pt}_{0.1}\text{Cu}_{0.9}$, which are 80 to 120 nm in size. This discrepancy may be due to the crude model to estimate the DMI in a mixture. Figure 5 shows the color mapping of out-of-plane magnetization at various K_u ($0.5, 0.7,$ and 0.9 mJ/m^3) and interfacial-DMI ($1.5, 3.0, 4.5,$ and 6.0 mJ/m^2), with blue regions corresponding to up magnetic moments and red regions corresponding to down magnetic moments. Robust shapes of skyrmions are found in this Mn_4N heterostructures throughout various K_u and interfacial-DMI, even with the presence of interfacial mixings. This is critical for any potential future for using Mn_4N in spintronics applications. Overall, these results verify the reliability of Mn_4N to host skyrmions, despite the existence of magnetic dead layers, and confirm the potential of using Mn_4N in skyrmion-based devices.

IV. CONCLUSION

Ferrimagnetic Mn_4N thin films are recently recognized as promising skyrmionic materials due to thermal stability and the ability to host small skyrmions. These material attributes prompted us to study interfacial mixing effect in $\text{MgO}/\text{Mn}_4\text{N}/(\text{Pt}-\text{Cu})$ heterostructures. From X-ray photoelectron spectroscopy, elemental mixings were revealed at both $\text{MgO}/\text{Mn}_4\text{N}$ and $\text{Mn}_4\text{N}/\text{Pt}$ interface. These mixing regions are about 5 nm thick, comparable to room temperature deposition. Using polarized neutron reflectometry, we found that these interface regions exhibit essentially zero magnetization. To address the effect of these inhomogeneities on the potential of using Mn_4N in spintronic devices, micromagnetic simula-

tions were employed to investigate skyrmions in Mn_4N . Simulated skyrmions were found to be robust at room temperature, despite the existence of magnetic dead layers. These results confirm that Mn_4N is a promising material for next-generation memory and logic devices.

ACKNOWLEDGMENTS

This work was partially supported by the DARPA Topological Excitations in Electronics (TEE) program (grant D18AP00009). The content of the information does not necessarily reflect the position or the policy of the Government, and no official endorsement should be inferred. Approved for public release; distribution is unlimited. The Phi VersaProbe III XPS used for acquiring the data was provided through the NSF-MRI Award #1626201.

DATA AVAILABILITY STATEMENT

The data that support the findings of this study are available from the corresponding author upon reasonable request.

- ¹B. N. Engel, C. D. England, R. A. Van Leeuwen, M. H. Wiedmann, and C. M. Falco, "Interface magnetic anisotropy in epitaxial superlattices," *Phys. Rev. Lett.* **67**, 1910–1913 (1991).
- ²N. Nakajima, T. Koide, T. Shidara, H. Miyauchi, H. Fukutani, A. Fujimori, K. Iio, T. Katayama, M. Nývlt, and Y. Suzuki, "Perpendicular magnetic anisotropy caused by interfacial hybridization via enhanced orbital moment in Co/Pt multilayers: Magnetic circular x-ray dichroism study," *Phys. Rev. Lett.* **81**, 5229–5232 (1998).
- ³H. X. Yang, M. Chshiev, B. Dieny, J. H. Lee, A. Manchon, and K. H. Shin, "First-principles investigation of the very large perpendicular magnetic anisotropy at Fe/MgO and Co/MgO interfaces," *Phys. Rev. B* **84**, 054401 (2011).
- ⁴B. Dieny and M. Chshiev, "Perpendicular magnetic anisotropy at transition metal/oxide interfaces and applications," *Rev. Mod. Phys.* **89**, 025008 (2017).
- ⁵J. L. Leal and M. H. Kryder, "Spin valves exchange biased by $\text{Co}/\text{Ru}/\text{Co}$ synthetic antiferromagnets," *Journal of Applied Physics* **83**, 3720–3723 (1998), <https://doi.org/10.1063/1.366597>.
- ⁶S. Parkin, X. Jiang, C. Kaiser, A. Panchula, K. Roche, and M. Samant, "Magnetically engineered spintronic sensors and memory," *Proceedings of the IEEE* **91**, 661–680 (2003).
- ⁷R. A. Duine, K.-J. Lee, S. S. P. Parkin, and M. D. Stiles, "Synthetic antiferromagnetic spintronics," *Nature Physics* **14**, 217–219 (2018).
- ⁸W. Legrand, D. Maccariello, F. Ajejas, S. Collin, A. Vecchiola, K. Bouzehouane, N. Reyren, V. Cros, and A. Fert, "Room-temperature stabilization of antiferromagnetic skyrmions in synthetic antiferromagnets," *Nature Materials* **19**, 34–42 (2020).
- ⁹I. Dzyaloshinsky, "A thermodynamic theory of "weak" ferromagnetism of antiferromagnetics," *J. Phys. Chem. Solids* **4**, 241–255 (1958).
- ¹⁰T. Moriya, "Anisotropic superexchange interaction and weak ferromagnetism," *Phys. Rev.* **120**, 91–98 (1960).
- ¹¹A. Hrabec, N. A. Porter, A. Wells, M. J. Benitez, G. Burnell, S. McVitie, D. McGrouther, T. A. Moore, and C. H. Marrows, "Measuring and tailoring the dzyaloshinskii-moriya interaction in perpendicularly magnetized thin films," *Phys. Rev. B* **90**, 020402 (2014).
- ¹²H. Yang, A. Thiaville, S. Rohart, A. Fert, and M. Chshiev, "Anatomy of dzyaloshinskii-moriya interaction at Co/Pt interfaces," *Phys. Rev. Lett.* **115**, 267210 (2015).
- ¹³M. Belmeguenai, J.-P. Adam, Y. Roussigné, S. Eimer, T. Devolder, J.-V. Kim, S. M. Cherif, A. Stashkevich, and A. Thiaville, "Interfacial dzyaloshinskii-moriya interaction in perpendicularly magnetized

- Pt/Co/AIO₃ ultrathin films measured by Brillouin light spectroscopy,” *Phys. Rev. B* **91**, 180405 (2015).
- ¹⁴Y. Quessab, J.-W. Xu, C. T. Ma, W. Zhou, G. A. Riley, J. M. Shaw, H. T. Nembach, S. J. Poon, and A. D. Kent, “Tuning interfacial Dzyaloshinskii-Moriya interactions in thin amorphous ferrimagnetic alloys,” *Sci. Rep.* **10**, 7447 (2020).
- ¹⁵P. F. Carcia, S. I. Shah, and W. B. Zeper, “Effect of energetic bombardment on the magnetic coercivity of sputtered Pt/Co thin-film multilayers,” *Applied Physics Letters* **56**, 2345–2347 (1990), <https://doi.org/10.1063/1.102912>.
- ¹⁶Y.-H. Wang, W.-C. Chen, S.-Y. Yang, K.-H. Shen, C. Park, M.-J. Kao, and M.-J. Tsai, “Interfacial and annealing effects on magnetic properties of CoFeB thin films,” *Journal of Applied Physics* **99**, 08M307 (2006), <https://doi.org/10.1063/1.2176108>.
- ¹⁷S. Y. Jang, S. H. Lim, and S. R. Lee, “Magnetic dead layer in amorphous CoFeB layers with various top and bottom structures,” *Journal of Applied Physics* **107**, 09C707 (2010), <https://doi.org/10.1063/1.3355992>.
- ¹⁸J. Li, Z. Y. Wang, A. Tan, P.-A. Glans, E. Arenholz, C. Hwang, J. Shi, and Z. Q. Qiu, “Magnetic dead layer at the interface between a Co film and the topological insulator Bi₂Se₃,” *Phys. Rev. B* **86**, 054430 (2012).
- ¹⁹B. Hebler, A. Hassdenteufel, P. Reinhardt, H. Karl, and M. Albrecht, “Ferrimagnetic tb–fe alloy thin films: Composition and thickness dependence of magnetic properties and all-optical switching,” *Frontiers in Materials* **3** (2016), 10.3389/fmats.2016.00008.
- ²⁰C. T. Ma, B. J. Kirby, X. Li, and S. J. Poon, “Thickness dependence of ferrimagnetic compensation in amorphous rare-earth transition-metal thin films,” *Applied Physics Letters* **113**, 172404 (2018), <https://doi.org/10.1063/1.5050626>.
- ²¹S. Laureti, A. Gerardino, F. D’Acapito, D. Peddis, and G. Varvaro, “The role of chemical and microstructural inhomogeneities on interface magnetism,” *Nanotechnology* **32**, 205701 (2021).
- ²²J.-G. J. Zhu and C. Park, “Magnetic tunnel junctions,” *Materials Today* **9**, 36–45 (2006).
- ²³S. Ghosh, T. Komori, A. Hallal, J. Peña Garcia, T. Gushi, T. Hirose, H. Mitarai, H. Okuno, J. Vogel, M. Chshiev, J.-P. Attané, L. Vila, T. Suemasu, and S. Pizzini, “Current-driven domain wall dynamics in ferrimagnetic nickel-doped Mn₄N films: Very large domain wall velocities and reversal of motion direction across the magnetic compensation point,” *Nano Letters* **21**, 2580–2587 (2021).
- ²⁴W. J. Takei, R. R. Heikes, and G. Shirane, “Magnetic Structure of Mn₄N-Type Compounds,” *Phys. Rev.* **125**, 1893–1897 (1962).
- ²⁵M. Meinert, “Exchange interactions and Curie temperatures of the tetrametal nitrides Cr₄N, Mn₄N, Fe₄N, Co₄N, and Ni₄N,” *Journal of Physics: Condensed Matter* **28**, 056006 (2016).
- ²⁶Y. Yasutomi, K. Ito, T. Sanai, K. Toko, and T. Suemasu, “Perpendicular magnetic anisotropy of Mn₄N films on MgO(001) and SrTiO₃(001) substrates,” *J. Appl. Phys.* **115**, 17A935 (2014).
- ²⁷K. Kabara and M. Tsunoda, “Perpendicular magnetic anisotropy of Mn₄N films fabricated by reactive sputtering method,” *J. Appl. Phys.* **117**, 17B512 (2015).
- ²⁸A. Foley, J. Corbett, A. Khan, A. L. Richard, D. C. Ingram, A. R. Smith, L. Zhao, J. C. Gallagher, and F. Yang, “Contribution from Ising domains overlapping out-of-plane to perpendicular magnetic anisotropy in Mn₄N thin films on MgO(001),” *J. Magn. Magn. Mater.* **439**, 236–244 (2017).
- ²⁹T. Hirose, T. Komori, T. Gushi, A. Anzai, K. Toko, and T. Suemasu, “Strong correlation between uniaxial magnetic anisotropic constant and in-plane tensile strain in Mn₄N epitaxial films,” *AIP Adv.* **10**, 025117 (2020).
- ³⁰T. Hirose, T. Komori, T. Gushi, K. Toko, and T. Suemasu, “Perpendicular magnetic anisotropy in ferrimagnetic Mn₄N films grown on (LaAlO₃)_{0.3}(Sr₂TaAlO₆)_{0.7}(001) substrates by molecular beam epitaxy,” *Journal of Crystal Growth* **535**, 125566 (2020).
- ³¹S. Isogami, K. Masuda, and Y. Miura, “Contributions of magnetic structure and nitrogen to perpendicular magnetocrystalline anisotropy in antiperovskite ε–Mn₄N,” *Phys. Rev. Materials* **4**, 014406 (2020).
- ³²W. Zhou, C. T. Ma, T. Q. Hartnett, P. V. Balachandran, and S. J. Poon, “Rare-earth-free ferrimagnetic Mn₄N sub-20 nm thin films as potential high-temperature spintronic material,” *AIP Adv.* **11**, 015334 (2021).
- ³³C. T. Ma, T. Q. Hartnett, W. Zhou, P. V. Balachandran, and S. J. Poon, “Tunable magnetic skyrmions in ferrimagnetic Mn₄N,” *Applied Physics Letters* **119**, 192406 (2021), <https://doi.org/10.1063/5.0066375>.
- ³⁴M. Tokaç, S. A. Bunyaev, G. N. Kakazei, D. S. Schmool, D. Atkinson, and A. T. Hindmarch, “Interfacial structure dependent spin mixing conductance in cobalt thin films,” *Phys. Rev. Lett.* **115**, 056601 (2015).
- ³⁵V. P. Amin, J. Zemen, and M. D. Stiles, “Interface-generated spin currents,” *Phys. Rev. Lett.* **121**, 136805 (2018).
- ³⁶L. Jin, K. Jia, D. Zhang, B. Liu, H. Meng, X. Tang, Z. Zhong, and H. Zhang, “Effect of interfacial roughness spin scattering on the spin current transport in YIG/NiO/Pt heterostructures,” *ACS Applied Materials & Interfaces* **11**, 35458–35467 (2019).
- ³⁷M. Li, D. Zhang, L. Jin, B. Liu, Z. Zhong, X. Tang, H. Meng, Q. Yang, L. Zhang, and H. Zhang, “Interfacial chemical states and recoverable spin pumping in YIG/Pt,” *Applied Physics Letters* **118**, 042406 (2021), <https://doi.org/10.1063/5.0035640>.
- ³⁸B. Maranville, W. Ratcliff II, and P. Kienzle, “*reductus*: a stateless Python data reduction service with a browser front end,” *Journal of Applied Crystallography* **51**, 1500–1506 (2018).
- ³⁹B. Kirby, P. Kienzle, B. Maranville, N. Berk, J. Krycka, F. Heinrich, and C. Majkrzak, “Phase-sensitive specular neutron reflectometry for imaging the nanometer scale composition depth profile of thin-film materials,” *Current Opinion in Colloid & Interface Science* **17**, 44–53 (2012).
- ⁴⁰C. F. Majkrzak, K. V. O’Donovan, and N. F. Berk, *Neutron Scattering from Magnetic Materials* (Elsevier, Amsterdam, 2006) p. 397–471.
- ⁴¹M. J. Donahue, “OOMMF user’s guide, version 1.0,” *Tech. Rep.* (1999).
- ⁴²X. Shen, A. Chikamatsu, K. Shigematsu, Y. Hirose, T. Fukumura, and T. Hasegawa, “Metallic transport and large anomalous Hall effect at room temperature in ferrimagnetic Mn₄N epitaxial thin film,” *Appl. Phys. Lett.* **105**, 072410 (2014).
- ⁴³B. B. Maranville, A. Green, and P. A. Kienzle, “Distributed error-function roughness in reflectometry fitting program,” (2018).
- ⁴⁴B. J. Kirby, L. Fallarino, P. Riego, B. B. Maranville, C. W. Miller, and A. Berger, “Nanoscale magnetic localization in exchange strength modulated ferromagnets,” *Phys. Rev. B* **98**, 064404 (2018).